Dual-projection optical diffusion tomography

Vadim A. Markel and John C. Schotland

Departments of Radiology and Bioengineering, University of Pennsylvania, Philadelphia, Pennsylvania 19104

Received March 5, 2004

We propose a new approach to optical diffusion tomography that incorporates two orthogonal projections. All the data obtained in a double projection measurement are treated simultaneously. The second projection improves image quality due to the fact that the depth and transverse directions are interchanged. An image reconstruction algorithm is derived and illustrated with simulations. It is shown that the spatial resolution of images improves by a factor of 4–5 due to the second projection. © 2004 Optical Society of America

OCIS codes: 170.0110, 170.3010, 170.3880.

Optical diffusion tomography (ODT) is an emerging biomedical imaging modality that utilizes near-infrared (NIR) light as a probe of biological tissue.[1] It is generally recognized that ODT has the potential to complement existing imaging methods and may have applications to breast imaging, functional brain mapping, and molecular imaging.[2] In the NIR spectral region light experiences relatively weak absorption but is strongly scattered in tissue. As a result, the inverse problem of ODT is ill posed. Consequently, the reconstructed images in ODT are of relatively low quality, which limits the clinical utility of this method.

Optimization of image quality in ODT has attracted significant attention (e.g., Refs. 3 and 4). However, the high computational complexity of the image reconstruction algorithms utilized in those studies necessitated the use of data sets with relatively small numbers of measurements (source–detector pairs). We recently introduced a family of image reconstruction algorithms that is free of this limitation.[5,6] With the use of these algorithms it was demonstrated that increasing the size of the data set can systematically improve image quality. We also showed that in the slab imaging geometry, which is often utilized for breast imaging, the transverse and depth resolutions are fundamentally different. The depth resolution is controlled by noise and the fact that the inverse problem is intrinsically ill posed.[6] In contrast, the transverse resolution is more stable in the presence of noise and scales as the minimum separation between the sources (detectors) and thus can potentially be very small compared to depth resolution.[5] This observation suggests that the use of measurements from dual projections (different orientations of the slab) should improve image quality by interchanging the depth and transverse directions. In this Letter we describe an image reconstruction method that combines the features of computationally efficient algorithms[5,6] with the use of dual projections. Using this approach, we demonstrate in numerical simulations that the addition of a second orthogonal projection can dramatically improve the spatial resolution and quality of reconstructed images.

We use the diffusion approximation to describe the propagation of NIR light in tissue.[1] The density of electromagnetic energy u is assumed to obey the stationary diffusion equation $D_0\nabla^2 u(\mathbf{r}) - \alpha(\mathbf{r})u(\mathbf{r}) + S(\mathbf{r}) = 0$, where D_0 and $\alpha(\mathbf{r})$ are the diffusion and absorption coefficients, respectively, and S is an appropriate source function. For simplicity we assume below that the diffusion coefficient $D(\mathbf{r}) = D_0$ is constant. The diffusion equation is supplemented by an expression for the measurable intensity that has the form $I = (4\pi/3)(u - l^*\hat{\mathbf{s}}\cdot\nabla u)$, where $l^* = 3D_0/c$ is the transport mean free path and $\hat{\mathbf{s}}$ is the direction in which the energy flux is measured. The inverse problem of ODT is to find the spatial distributions of α inside the tissue from surface measurements of intensity I. This inverse problem is nonlinear.[1] We perform a standard linearization assuming that $\alpha(\mathbf{r}) = \alpha_0 + \delta\alpha(\mathbf{r})$, where α_0 is the known background value of the absorption coefficient and $\delta\alpha$ is a small fluctuating part. Then the measured signal $\phi(\mathbf{r}_s, \mathbf{r}_d)$ can be related to $\delta\alpha$ by the linear integral equation

$$\phi(\mathbf{r}_s, \mathbf{r}_d) = \int \Gamma_A(\mathbf{r}_s, \mathbf{r}_d; \mathbf{r})\delta\alpha(\mathbf{r})\mathrm{d}^3 r\,, \tag{1}$$

where $\mathbf{r}_s$ and $\mathbf{r}_d$ are the positions of the source and the detector, respectively, and the kernel Γ can be expressed in terms of Green's function $G_0(\mathbf{r}, \mathbf{r}')$ of the diffuse equation in a medium with $\alpha = \alpha_0$ and $D = D_0$ and appropriate boundary conditions.[7]

Since only one optical coefficient (namely, $\delta\alpha$) is recovered in this case, stationary (dc) measurements are sufficient.[7,8] Second, we assume that the measurements are performed in an infinite medium (free boundary conditions). Then kernel Γ is given by $\Gamma(\mathbf{r}_s, \mathbf{r}_d; \mathbf{r}) = G_0(\mathbf{r}_s, \mathbf{r})G_0(\mathbf{r}, \mathbf{r}_d)$. Note that these assumptions are not fundamental and can be easily avoided in practical applications. The details for general boundary conditions and simultaneous reconstruction of $\delta\alpha$ and δD, as well as the results for more than two different projections, will be published elsewhere.

In the slab geometry illustrated in Fig. 1 Green's function G_0 can be expressed as a one-dimensional Fourier integral of the form

$$G_0(x, y, z; x', y', z') = \int_{-\infty}^{\infty} \frac{\mathrm{d}\zeta}{2\pi} \exp[i\zeta(z' - z)] \times g(\zeta; x' - x, y' - y)\,. \tag{2}$$

0146-9592/04/172019-03$15.00/0

In the case of free boundaries considered here, $g(\zeta; x' - x, y' - y) = (1/2\pi D_0)K_0\{Q(\zeta)[(x - x')^2 + (y - y')^2]^{1/2}\}$, where $Q(\zeta) = (\zeta^2 + k_{\mathrm{diff}}^2)^{1/2}$, $k_{\mathrm{diff}} = (\alpha_0/D_0)^{1/2}$ is the diffuse wave number, and $K_0(x)$ is the modified Bessel function of the second kind.

We now turn to the derivation of an image reconstruction algorithm that utilizes simultaneously the data obtained from two orthogonal projections shown in Fig. 1. This is in contrast with previous studies in which multiple projections in optical tomography have been used in conjunction with a modified version of x-ray backprojection tomography with phenomenological corrections introduced to compensate for scattering.[9,10] The slab can take one of two possible positions, and the reconstruction is performed in the shaded square region, which is not perturbed by rotations of the slab. Let the position of the sources and detectors on the incident and exit surfaces of the slab be denoted by (x_s, y_s, z_s) and (x_d, y_d, z_d), respectively. For the first orientation of the slab we have $x_s = -L/2$, $x_d = L/2$, whereas y_s, z_s and y_d, z_d take multiple values: $y_s(n_s) = -(N_s - 1)h/2 + (n_s - 1)h$, $y_d(n_d) = -(N_d - 1)h/2 + (n_d - 1)h$, $z_s(m_s) = m_s h$, and $z_d(m_d) = m_d h$, where $n_{s,d} = 1, \ldots, N_{s,d}$ and $m_{s,d} = 0, \pm 1, \pm 2, \ldots$. Here h is the intersource (interdetector) separation of the lattice step. Thus for each given $x - y$ cross section there are $N_{s,d}$ sources or detectors equally spaced within window $W_{s,d} = (N_{s,d} - 1)h$. However, the system is infinite in the z direction. The latter requirement is necessary for mathematical consistency but cannot be fulfilled experimentally. However, because of the rapid exponential decay of diffuse waves, a finite window in the z direction is anticipated to be sufficient for data collection.[5] For the second orientation of the slab, $z_{s,d}$ take the same values as above, but $x_{s,d}$ and $y_{s,d}$ are mutually interchanged. Now we have $y_s = L/2$ and $y_d = -L/2$ while $x_s(n_s) = -(N_s - 1)h/2 + (n_s - 1)h$ and $x_d(n_d) = -(N_d - 1)h/2 + (n_d - 1)h$.

Now we use expansion (2) and Fourier transform main integral equation (1) with respect to variables z_s and z_d. We then define the Fourier-transformed data function as

$$\tilde{\phi}(x_s, y_s, q_s; x_d, y_d, q_d) = \sum_{m_s=-\infty}^{\infty} \sum_{m_d=-\infty}^{\infty} \phi(x_s, y_s, z_s; \times x_d, y_d, z_d)\exp\{i[q_s z_s(m_s) + q_d z_d(m_d)]\} \quad (3)$$

and a new data function $\psi_{k,n_s,n_d}(q)$ according to

$$\psi_{k,n_s,n_d}(q) = \begin{cases} \tilde{\phi}[-L/2, y_s(n_s), q/2; L/2, y_d(n_d), q/2], & \text{if } k = 1 \\ \tilde{\phi}[x_s(n_s), L/2, q/2; x_d(n_d), -L/2, q/2], & \text{if } k = 2 \end{cases}. \quad (4)$$

Here index $k = 1, 2$ labels the projection number. We substitute expansion (2) into Eq. (1) and apply Fourier transformation (3) and definition (4) to obtain

$$\psi_{k,n_s,n_d}(q) = \int_{-L/2}^{L/2} \mathrm{d}x \int_{-L/2}^{L/2} \mathrm{d}y \kappa_{k,n_s,n_d}(q; x, y)\delta\tilde{\alpha}(x, y; q), \quad (5)$$

where

$$\kappa_{k,n_s,n_d}(q; x, y) = \sum_{l=-\infty}^{\infty} \begin{cases} g\left[\frac{Q}{2} - \frac{2\pi l}{h}; -\frac{L}{2} - x, y_s(n_s) - y\right] g\left[\frac{Q}{2} + \frac{2\pi l}{h}; x - \frac{L}{2}, y - y_d(n_d)\right], & k = 1 \\ g\left[\frac{Q}{2} - \frac{2\pi l}{h}; x_s(n_s) - x, \frac{L}{2} - y\right] g\left[\frac{Q}{2} + \frac{2\pi l}{h}; x - x_d(n_d), y + \frac{L}{2}\right], & k = 2 \end{cases} \quad (6)$$

and $\delta\tilde{\alpha}(x, y; q)$ is the Fourier transform of $\delta\alpha(x, y, z)$ with respect to z defined by

$$\delta\tilde{\alpha}(x, y; q) = \int_{-\infty}^{\infty} \delta\alpha(x, y, z)\exp(iqz)\mathrm{d}z. \quad (7)$$

It can be seen that Eq. (5) is a set of independent integral equations parameterized by q. For a fixed value of q each integral equation can be discretized by replacing the integrals over $\mathrm{d}x$ and $\mathrm{d}y$ by Riemann sums. Thus we obtain a set of independent systems of linear algebraic equations for each q. Each of these systems can be solved by standard singular value decomposition methods to obtain $\delta\tilde{\alpha}(x, y; q)$. An approximation to the real-space function can then be recovered by the inverse Fourier transform:

$$\delta\alpha(x, y, z) = \int_{-\pi/h}^{\pi/h} \delta\tilde{\alpha}(x, y; q)\exp(-iqz)\frac{\mathrm{d}q}{2\pi}, \quad (8)$$

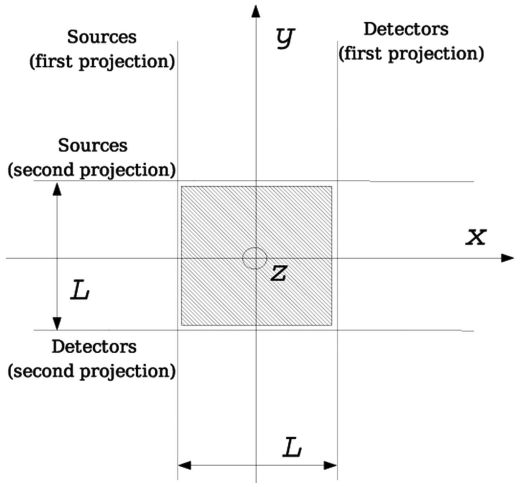

Fig. 1. Illustration of the reference frame used for the derivation of inversion formulas.

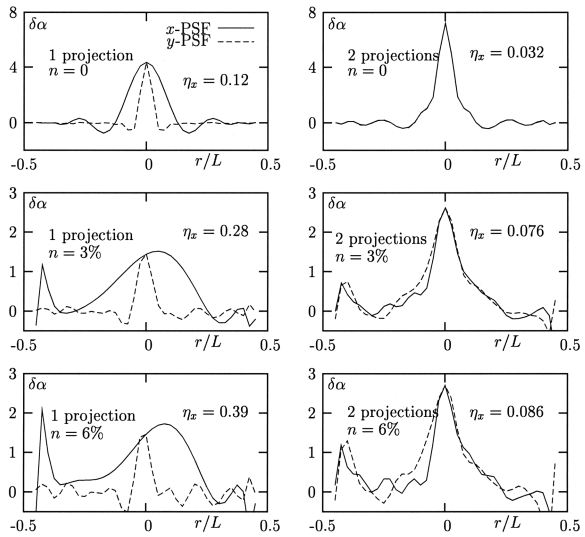

Fig. 2. PSFs in reconstructed images of a point absorber for single (left column) and double (right column) projection imaging and different levels of random Gaussian noise n. Image quality parameter η_x for the x PSFs is shown in each graph.

where we have assumed that $\delta\tilde{\alpha}(x, y; q)$ is band limited to the first Brillouin zone of the lattice of sources (detectors), namely, $-\pi/h < q \leq \pi/h$.[5]

Equations (5)–(8) are the mathematical formulation of the image reconstruction algorithm proposed in this Letter. The inversion is analytical in one dimension (z) and numerical in the two remaining dimensions (x and y). It is important to note that the reduction from the three-dimensional ODT problem to the two-dimensional problem leads to a dramatic decrease in computational complexity of numerical inversion {from $O[(W/h)^{12}]$ to $O[(W/h)^6]$, where parameter W/h can be of the order of 100 in certain applications}.

Point-spread functions (PSFs) are reconstructed images of a single-point (delta-function) absorber. Sample PSFs obtained by numerical implementation of the proposed algorithm at different levels of Gaussian random noise n are shown in Fig. 2. Here the forward data were calculated for a point (delta-function) absorber located at the center of a slab with thickness $L = \lambda_{\text{diff}} = 2\pi(D_0/\alpha_0)^{1/2}$. The windows in the plane perpendicular to the z axis were $W_s = W_d = 2L$, and the lattice step was $h = L/40$. PSFs are shown in the x and y directions corresponding to the depth and transverse directions, respectively, in the case of a single projection.

It is evident that the second projection significantly improves image quality. The improvement is especially pronounced at high noise levels. Note that the second projection makes the PSFs in the x and y directions approximately of the same width and shape. This helps remove distortions in the images that result from the substantially different shapes of the PSFs apparent in the one-projection case. Another advantage of two-projection imaging is that the PSFs do not change substantially when the absorber is moved closer to the measurement surfaces (data not shown). The dependence of the PSFs on depth in one-projection images is strong[6] and can result in severe image artifacts. To maintain the constant shape of the PSFs in the two-projection images (and high transverse resolution), window W must be significantly larger than L.

To quantify the quality of reconstructed images, we constructed a simple numerical measure. Let a function f be defined at N points in space: $f_i = f(\mathbf{r}_i)$, $i = 1, \ldots, N$. Assume that we know that the true values of this function, f_i^{target}, are zero everywhere except for $i = i_0$, whereas f_i is the reconstruction that only approximately coincides with f_i^{target}. Then we define $\eta = N^{-1}\sum_{i\neq i_0}(f_i/f_{i_0})^2$. Obviously, if f_i coincides exactly with the target, then $\eta = 0$. In general, η can be interpreted as the fraction of pixels for which the reconstructed result is substantially incorrect. The uncertainty in locating the position of the target can be estimated as $\delta r = hN\eta = \eta L$ for the PSFs shown in Fig. 2. It can seen that η decreases by a factor of 3–4 due to the second projection. For a noise-to-signal level of $n = 6\%$ the second projection results in reducing η by a factor of 4.5.

In summary, we have presented a computationally efficient algorithm for treating dual-projection data in ODT. The use of a second projection leads to significant improvement in image quality. In general, multiple-projection data can be collected in practice by filling the slab with matching fluid. Then either the sample can be rotated inside the device or the device itself can be rotated around the sample. This modality is well suited, for example, to imaging the breast and small animals.

This work was supported in part by the Air Force Office of Scientific Research under grant F41624-02-1-7001 and by the National Institutes of Health under grant P41RR0205. V. Markel's e-mail address is vmarkel@mail.med.upenn.edu, and J. Schotland's is schotland@seas.upenn.edu.

References

1. S. R. Arridge, Inverse Probl. **15,** R41 (1999).
2. D. J. Hawrysz and E. M. Sevick-Muraca, Neoplasia **2,** 388 (2000).
3. B. W. Pogue, T. O. McBride, U. L. Ostererg, and K. D. Paulsen, Opt. Express **4,** 270 (1999), http://www.opticsexpress.org.
4. J. P. Culver, V. Ntziachristos, M. J. Holboke, and A. G. Yodh, Opt. Lett. **26,** 701 (2001).
5. V. A. Markel and J. C. Schotland, Appl. Phys. Lett. **81,** 1180 (2002).
6. V. A. Markel and J. C. Schotland, J. Opt. Soc. Am. A **20,** 890 (2003).
7. V. A. Markel and J. C. Schotland, J. Opt. Soc. Am. A **19,** 558 (2002).
8. S. R. Arridge and W. R. B. Lionhart, Opt. Lett. **23,** 882 (1998).
9. S. B. Colak, D. G. Papaioannou, G. W. Hooft, M. B. van der Mark, H. Schomberg, J. C. J. Paasschens, J. B. M. Melissen, and N. A. A. J. van Asten, Appl. Opt. **36,** 180 (1997).
10. C. L. Matson and H. L. Liu, J. Opt. Soc. Am. A **16,** 1254 (1999).